Multiscale characterisation of AlSi9Cu3(Fe) die casting alloys after Cu, Mg, Zn and Sr addition

F. Sanna, A. Fabrizi, S. Ferraro, G. Timelli, P. Ferro, F. Bonollo

The Al-Si alloys are the most diffused foundry light alloys and now constitute 90% of the Al alloys used in the automotive sector. Among the industrial processes for the production of Al alloy components, the high pressure die casting is the most widespread technology. This paper presents the influence of different alloying elements such as Cu, Mg, Zn and Sr on the microstructure and mechanical properties of an AlSi9Cu3(Fe) die casting alloy. The metallographic analysis carried out by optical, scanning and transmission electron microscopy allowed to evaluate, at different scales, the size of the primary crystals of α-Al and the porosity too, as well as to identify the different intermetallic phases distributed in the microstructure. Hardness, microhardness and static tensile testing were also performed on the different alloys, and the experimental results were correlated with the different concentrations of the alloying elements.

Keywords: Aluminium alloys; HPDC; AlSi9Cu3(Fe); Cu; Mg; Zn; Sr; Microstructure; Mechanical properties; Steering gearbox.

INTRODUCTION

It is well known how, in the last two decades, automotive manufacturers have increased their attention to the production of lighter vehicles in order to satisfy the increasing demand of reducing fuel consumption and pollutant emissions. This trend resulted in a greater use of Al alloys for the production of structural components such as engine blocks and heads, brake calipers, wheels, pistons and steering gearboxes, historically produced by ferrous alloys. Among the Al-based alloys, the Al-Si foundry alloys are probably the most diffused. Their success is primarily due to the combination of excellent physical and chemical characteristics such as lightness and corrosion resistance, with a high specific strength, excellent castability, and low volume shrinkage during solidification. Further, the high production volume required by car manufacturers imposed the use of technologies with lower production cycle: for this reason, most of the Al-Si alloy components are produced by high pressure die casting (HPDC) process. This technology allows to obtain quickly and economically components with complex geometries and high quality surface [1]. However, the HPDC induces the formation of defects such as oxide films, shrinkage and air/gas porosity, which are difficult to be eliminated due to the limits of the process itself [2,3]. Casting defects can cause a structural weakening and a loss of performance of the die casting. Therefore, the use of HPDC is actually limited for safety components.

Several studies showed how the final mechanical properties are strictly related not only to the presence of defects, but also to the initial chemical composition of the alloy [4-6]. By using a more efficient melting practice and by improving the component design, it is possible to reduce the level of defects, thereby increasing the strength of the casting. The mechanical properties can also be significantly increased by controlling microstructural parameters such as the distance between the secondary dendrite arms (SDAS), the grain size, the shape and the distribution of the Al-Si eutectic, and the volume fraction of the intermetallic phases. These microstructural characteristics depend not only on the solidification condition, but they are closely related to the initial chemical composition of the alloy [7,8]. Alloying elements, such as Cu, Mg, Si, Zn, Fe, Mn, normally present in die casting alloys, can influence the microstructure and consequently the mechanical properties. The addition of modifying elements, such as Na and Sr, is a common foundry practice in the produc-

F. Sanna, A. Fabrizi, S. Ferraro, G. Timelli, P. Ferro, F. Bonollo
University of Padova,
Department of Management and Engineering,
Stradella S. Nicola, 3, I-36100 Vicenza, Italy.
Corresponding author:
Tel.: 00 39 0444 998769; fax. 00 39 0444 998889.
E-mail address: timelli@gest.unipd.it (G. Timelli)

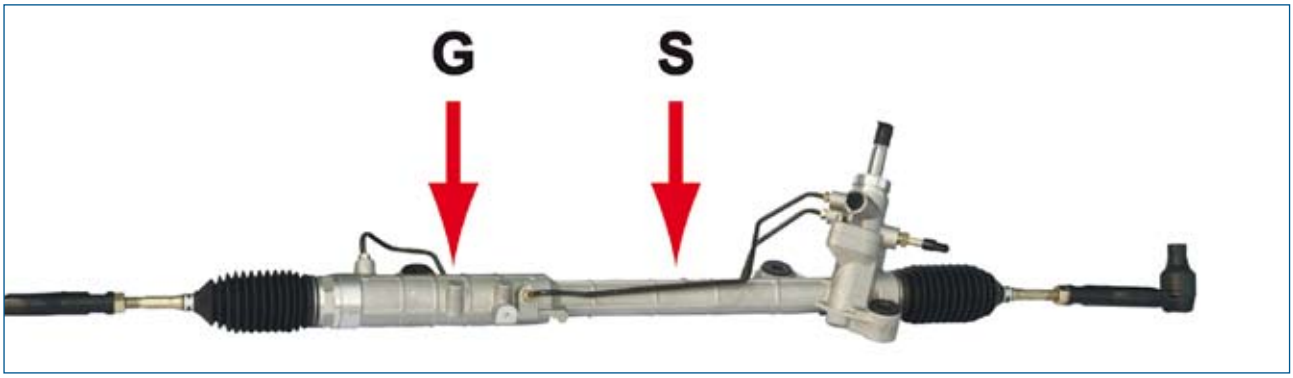

Fig. 1 - Example of a steering gearbox produced by Al die casting alloy; in the present work samples were drawn from the regions indicated by arrows, which present a thin (S) and thick (G) wall thickness, respectively.

Fig. 1 - Esempio di idroguida prodotta in lega di alluminio pressocolata; le frecce indicano le zone di prelievo dei saggi a spessore di parete sottile (S) e grossolana (G).

Alloy	Si	Fe	Cu	Mg	Sr	Zn	Cr	Ni	Ti	Pb	Mn	Al
0 (EN AC-46000)	9.27	0.86	2.45	0.24	0.0001	1.21	0.03	0.14	0.05	0.10	0.21	bal.
A	9.62	0.84	2.25	0.24	**0.0133**	1.06	0.06	0.12	0.04	0.09	0.22	bal.
B	9.91	0.84	2.33	0.46	**0.0153**	1.08	0.06	0.12	0.04	0.09	0.21	bal.
C	9.70	0.84	**4.30**	**0.48**	**0.0159**	1.08	0.07	0.11	0.04	0.09	0.21	bal.
D	9.72	0.84	**3.49**	**0.68**	**0.0162**	1.07	0.06	0.11	0.05	0.09	0.21	bal.
E	8.30	0.81	1.89	0.22	**0.0350**	3.99	0.03	0.11	0.05	0.12	0.21	bal.

Tab. 1 - Chemical composition of the experimental alloys (wt.%).

Tab. 1 - Composizione chimica delle diverse leghe analizzate (%pond).

tion of components realized by gravity and low pressure casting processes; these elements lead to the reduction of the size and aspect ratio of the eutectic Si particles and determine an increase of ductility [9]. Cu, Zn and Mg are usually added in primary alloys to increase the mechanical strength, especially if a post-casting heat treatment is required [10]. The addition of Si, up to the concentration of about 12%, improves the castability of the alloy and reduces the volumetric shrinkage during solidification [11]. Iron in Al-Si alloys combines with other elements to form complex intermetallic compounds with various morphologies. The β-Al_5FeSi phase, with a plate-like morphology, causes a deterioration of the mechanical properties, in particular the ductility and the toughness [12-15]; while the α-$Al_{15}(Fe, Mn)_2Si_3$ phase induces a lower decay of the properties due to a more compact morphology (Chinese Script) that reduces the stress concentration. In spite Fe is generally considered an impurity and a deleterious element, this is intentionally added in Al die casting alloys (e.g. >0.8 wt.%) to facilitate the release of the casting from the die [16]. The Mn is added to control the morphology of the Fe-rich phases. While increasing the volume fraction of the Fe-bearing particles, the Mn promotes the formation of a proeutectic α phase with a Chinese script morphology [17,18].

In the automotive field a plurality of characteristics is generally required, which can be hardly satisfied with the use of a standard secondary Al alloy. This work is aimed to investigate the role of some alloying elements such as Cu, Mg, Zn and Sr on the microstructure and mechanical properties of a secondary AlSi9Cu3(Fe) die casting alloy used for the production of automotive structural components.

MATERIAL AND EXPERIMENTAL PROCEDURE

Alloys and casting procedure

The analysed component is a diecast steering gearbox, similar to that illustrated in Figure 1, which is normally produced with a standard AlSi9Cu3(Fe) alloy (EN AC-46000), referred here as a base-line (Alloy 0). Different amounts of Cu, Mg, Zn and Sr were systematically added to the standard alloy in order to produce other five alloys (Alloys A-E). The chemical composition of each alloy is shown in Table 1.

An EN AB-46000 alloy (equivalent to the US designation A380) was supplied as commercial ingots, which were gas pre-heated at 250-300°C in a StrikoWestofen furnace with a capacity of 1700 kg/h, and subsequently brought to the melting temperature at about 720°C. The molten metal was tapped from the furnace and N-degassed for 3 min. During degassing, the alloying elements, in the form of master alloy (Al-10Zn, Al-10Sr) or pure metals (Cu, Mg), were added. The obtained alloys were transferred to a Westomat® holding furnace with a holding temperature of ~700°C. Casting was carried out on an Italpresse 13.2 MN locking force cold chamber HPDC machine. The shot

sleeve had a length of 400 mm and an outer diameter of 190 mm, while the piston had a diameter of 120 mm. The process parameters were kept constant during the whole experimental trials. The weight of the casting is 5.6 kg, and it is generally removed from the die at ~200°C and subsequently cooled in a water bath at a temperature of 30 ± 5°C to reach the final temperature of 70-80°C. The castings produced with the alloy E were subsequently artificially aged in an electric furnace at 80°C for 10 hours and were therefore similar to a T5-condition.

Microstructural and mechanical characterisation

Castings produced with the different alloys, with the exception of the alloy E, were stored at room temperature for about five months before being analysed and were therefore similar to a T1-condition. In order to verify the presence of macro-defects, the steering gearboxes were analysed by liquid penetrant testing and radioscopic investigation with a Bosello SRE 80 industrial machine equipped with an Hamamatsu microfocus X-ray.

Samples were drawn from 2 regions with different wall thickness (about 6 and 14 mm, respectively) to compare the effect of various cooling rates on the microstructure. These areas are indicated in Figure 1, named S (thin) and G (thick) respectively, and so called hereafter. Metallographic investigations were carried out by both optical microscope (OM, Leica DMLA) and field emission gun environmental scanning electron microscope (FEG-ESEM, FEI QUANTA 250) equipped with an energy-dispersive spectrometer (EDS, EDAX). In order to confirm the presence of some intermetallic phases, a study was carried out using a transmission electron microscope (TEM, JEOL JEM 2000 EX II). The micrographs were processed by image analysis software to measure SDAS values, the defect content, and the size and the shape of the different intermetallic compounds.

Hardness measurements was performed on ground and polished samples. Vickers microhardness measurements were carried out using a load of 0.005 kgf and a 15-second dwell period. Macro Brinell hardness measurements were also carried out by using a load of 62.5 kgf, according to the standard UNI EN ISO 6506-1:2006.

Static tensile testing was performed on specimens drawn from the central body of the steering gearbox according to the standard UNI EN ISO 6892-1:2009. Eight or more tensile tests were conducted for each alloy, and the mean mechanical properties were obtained considering the average of the four best values, excluding in this way the effect of a high defect content. The tensile tests were done on a MTS 858 Mini-Bionix machine. The crosshead speed used was 2 mm/min and the strain measured using a 25-mm extensometer.

RESULTS AND DISCUSSION

Defect characterization

The liquid penetrant testing allowed to verify the absence of surface defects. The X-ray analysis instead showed the

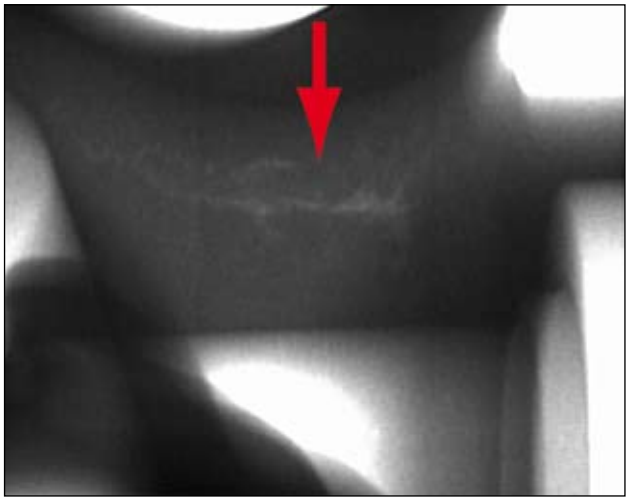

Fig. 2 - X-ray image of one end of the casting. The arrow indicates the presence of macroporosity.

Fig. 2 - Immagine ai Raggi-X di una estremità del getto. La freccia indica la presenza di una macroporosità.

presence of macroporosity, located in the regions of thick areas (Figure 2), corresponding to the hot spots of the casting. The amount and the size of porosity were estimated on the polished samples drawn from the castings. Porosity with small size (mean area ~200 μm^2), mainly due to entrapped air/gas or microshrinkage, was identified in samples with thin wall thickness (S). The samples with thick section (G) showed higher content of coarse pores, mainly due to macroshrinkage (mean area ~700 μm^2).

Figure 3 shows the porosity content as a function of the different alloy and wall thickness analysed. The thin sections evidence a relatively low defect amount, with a level of porosity almost constant throughout the alloys. In the thick sections, the porosity level seems to decrease by in-

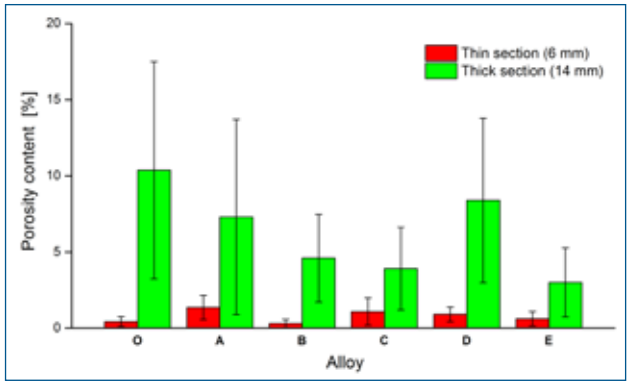

Fig. 3 - Porosity content in the castings produced with the different alloys, as estimated, respectively, from thin and thick sections of the casting. Standard deviations are given as error bars.

Fig. 3 - Percentuale di porosità valutata nei campioni sottili e grossolani di ogni lega. Le barre di errore rappresentano la deviazione standard.

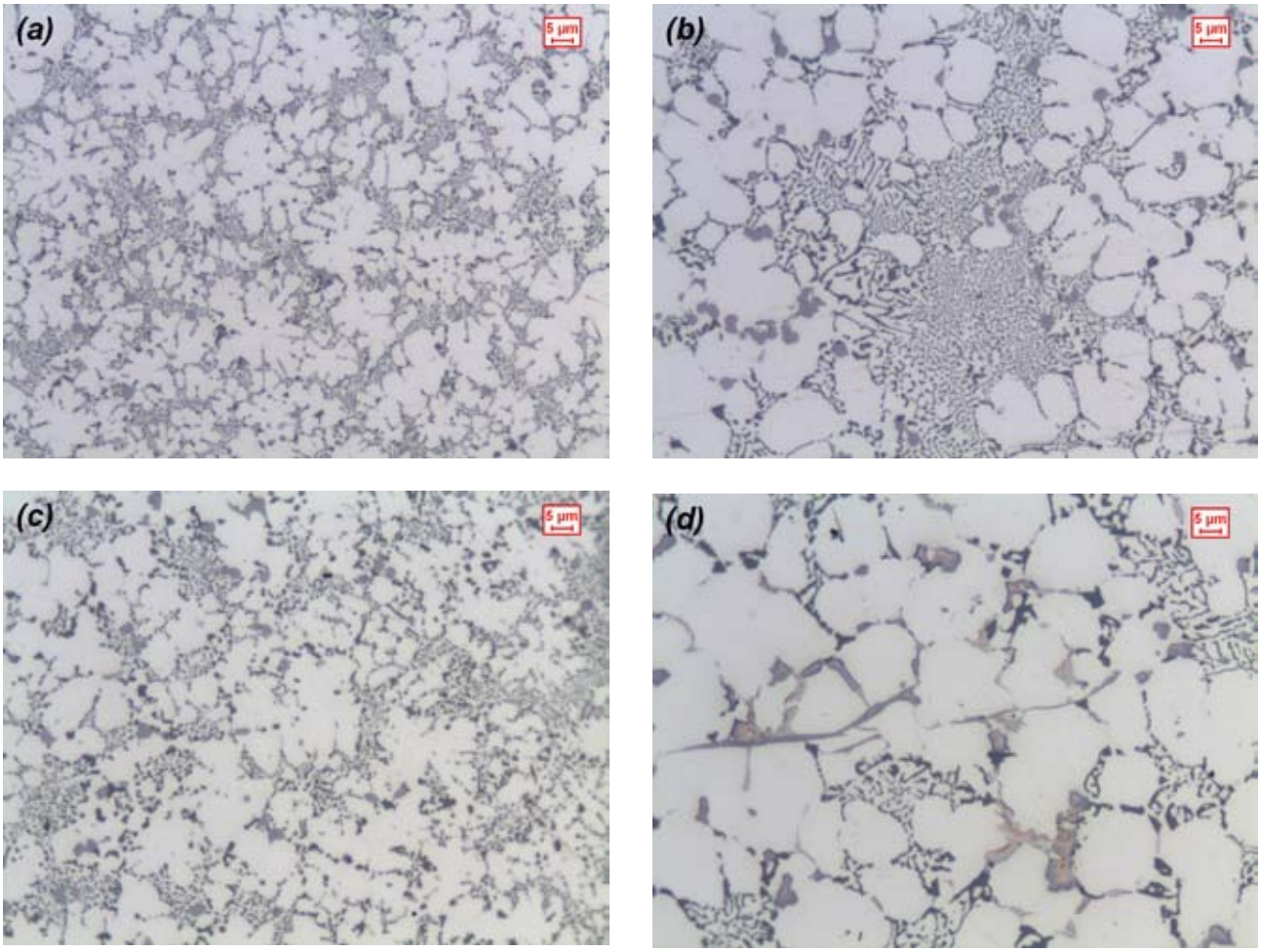

Fig. 4 - Microstructures at different positions of (a,b) thin and (c,d) thick wall thickness. The micrographs refer to (a,c) the casting surface and (b,d) the centre of the casting produced with alloy A.

Fig. 4 - Microstrutture delle sezioni a spessore sottile (a, b) e grossolano (c, d). Le micrografie si riferiscono alla superficie (a,c) e al cuore (b,d) del getto dei getti prodotti con la lega A.

creasing the solute content. Exception to this trend is represented by the alloy D with the highest Mg content (0.68 wt.%). The different defect content in these samples can be partially explained considering the different volumetric shrinkage of the alloys during solidification. The solidification shrinkage of Al die casting alloys varies definitely with the chemical composition and the content of the alloying elements, as reported in Ref. [19].

Macro- and microstructural investigations

SDAS analysis

The typical microstructures obtained from different positions of thin and thick sections are shown in Figure 4. The micrographs refer to the casting surface and the centre of the castings, respectively. The effect of the different solidification rate on the microstructural scale, i.e. SDAS, can be observed. The average values of SDAS, evaluated in the different alloys, are shown in Figure 5. The measurements were carried out both at the casting surface and at the centre of thin (Figure 5a) and thick sections (Figure 5b), respectively. In general, lower SDAS values were found at the casting surface, where almost a rapid solidification takes place. Due to the different heat exchange, SDAS at the centre of the thin sections are lower if compared to the values in the thick sections. The different cooling conditions between inner and outer edges, namely the areas in contact with the insert and the die respectively, can also be estimated from SDAS measurements (Figure 5).

These observations confirm how higher cooling rates, i.e. shorter solidification time, limits the dendrite growth and leads to the SDAS reduction [20-22]. Figure 5 also evidences how the SDAS variation is strictly connected to the initial chemical composition of the alloy. For a fixed solidification time, the value of SDAS varies by varying the content of alloying elements [7]. Recent studies [23] have shown that, in Al foundry alloys, the SDAS values decrease as the Si, Cu and Fe content increases. Moreover, the addition of Cu up to levels of 4.7 wt.% leads to a SDAS reduction of about 19% [24].

The experimental results can be modelled by the by Kirkwood and Feurer formulation [25,26]:

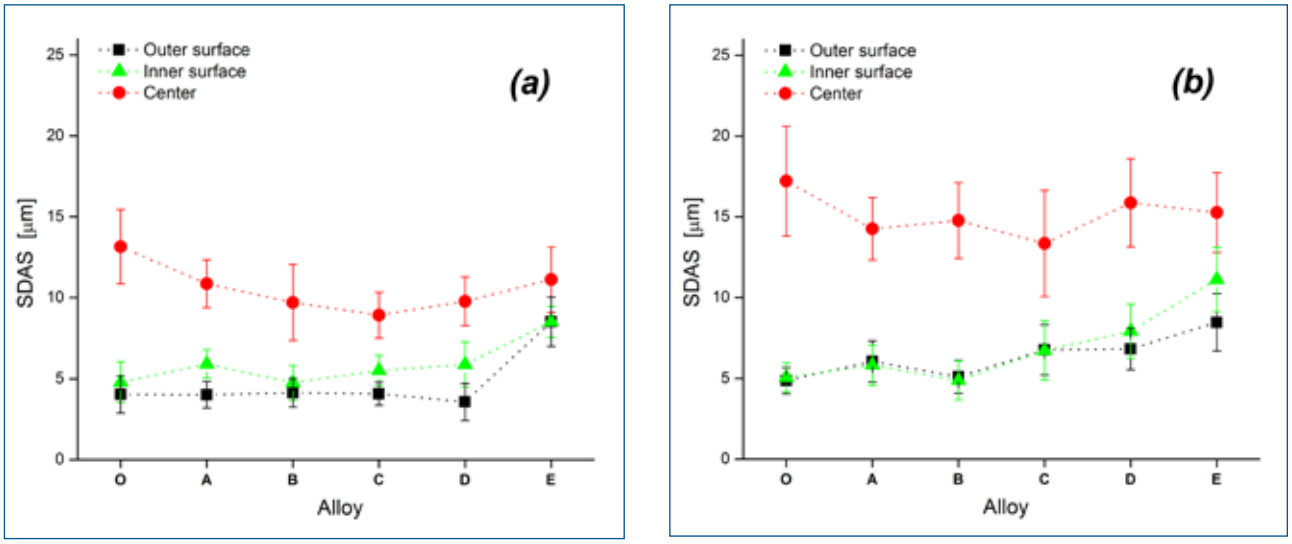

Fig. 5 - Mean SDAS values estimated at various regions of (a) thin and (b) thick sections from the castings produced with the different alloys. Standard deviations are given as error bars.

Fig. 5 - Andamento dello SDAS nelle diverse leghe prodotte per campioni con spessore di parete sottile (a) e grossolano (b). Le barre di errore rappresentano la deviazione standard.

$$SDAS = 5.5 \cdot \left(M \cdot t_s\right)^{1/3} \qquad (1)$$

where t_s is the solidification time and M is a coefficient that depends on the chemical composition. The extended formulation of M in eq. (1), in the case of a generic binary system, can evidence the influence of the initial chemical concentration on SDAS [25,27]:

$$M = \frac{\Gamma \cdot D \cdot \ln\left(\frac{C_t^m}{C_0}\right)}{m \cdot (1-k) \cdot \left(C_0 - C_t^m\right)} \qquad (2)$$

where Γ is the Gibbs-Thomson coefficient, D the diffusion coefficient, k the distribution coefficient, m the slope of the liquidus curve, C_0 and C_t^m are the initial and final composition of the liquid respectively.

Eutectic Si characterization

The average size (D_{eq}) of the eutectic Si particles measured at the centre of each section is shown in Figure 6. The corresponding values measured at the casting surface, not reported in the figure, are steady at ~0.5 µm, both as a function of the chemical composition and wall thickness. In the casting regions close to the die, due to high cooling rate, the nucleation mechanism prevails on the growth one, therefore promoting the formation of fine and fibrous eutectic Si. This modified microstructure appears identical to that obtained by chemical modification, despite the growth mechanism of the eutectic silicon is different [28,29]. Therefore, the effects of Sr modification on the eutectic Si are most evident at the centre of the thick sections, where higher solidification times occur.

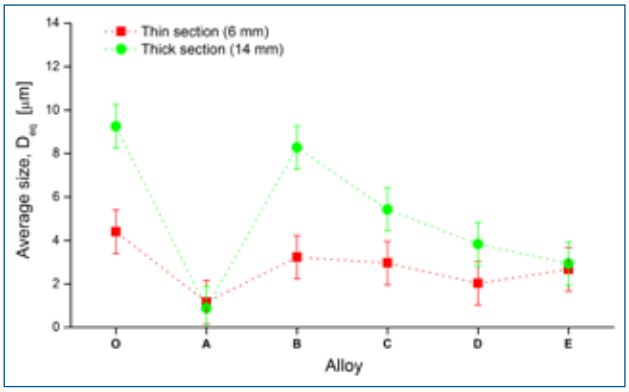

Figure 6. Average size (D_{eq}) of eutectic Si particles in the experimental alloys, as estimated in thin and thick sections of castings.

Figura 6. Andamento del diametro equivalente medio (D_{eq}) delle particelle di Si eutettico valutato nei campioni con spessore di parete sottile e grossolano.

In general, D_{eq} values are higher in the thick sections than in the thin ones, and the highest values were detected for the base-line AlSi9Cu3(Fe) alloy (alloy 0); the lowest values were instead obtained in the alloy A that is alloyed with 130 ppm Sr. The other experimental alloys, with the same, or higher, Sr content, do not reach the same level of eutectic Si refining. This can be due to a negative interaction between Cu, Mg and Zn with Sr, which may counteract the Sr-modification effect. This result seems to be in agreement with Ref. [30], where the reduction of the eutectic Si particles, obtained by adding 200 ppm Sr in an AlSi11Mg alloy, is counteracted by increasing the Mg content up to 0.45 wt.%.

Figure 7 shows the different morphology of the eutectic Si

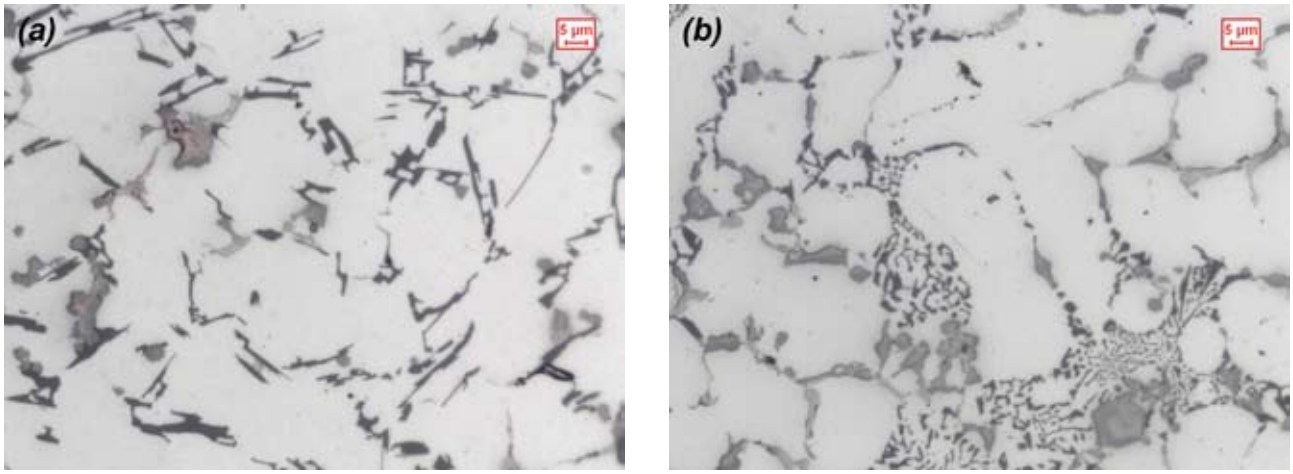

Fig. 7 - Micrographs in the middle of a thick section of (a) alloy 0 and (b) alloy A; eutectic Si is the dark grey phase.

Fig. 7 - Micrografie a cuore di un campione grossolano della lega 0 (a) e della lega A (b); il Si eutettico è la fase di colore grigio scuro.

particles in the base alloy (alloy 0) and Sr-added alloy (alloy A). The morphology distribution, such as the aspect ratio and the roundness, of the eutectic Si particles were also investigated and found to follow the three-parameters lognormal distribution in all the experimental alloys (Figure 8).
The morphology distributions of the eutectic Si become more spread after Sr addition (Figure 8), confirming what it is evident in Figure 7; the eutectic Si particles show a typical coarse plate-like morphology in alloy 0, while appear more fibrous and globular in the other Sr-modified alloys. In addition to the eutectic Si refinement, Sr is thus responsible for the morphological changes of the eutectic Si particles and this last behaviour, differently from the refining mechanism, seems to not be affected by the presence of other added elements (Cu, Mg, Zn).

Intermetallic compounds

A high amount of intermetallic compounds, with a polygonal shape and identified as α-$Al_{15}(Fe,Mn,Cr)_3Si_2$ by the EDS analysis, were observed in all the considered samples (Figure 9). This phase can also show a Chinese script morphology, depending on the Mn content [18,31]. However, this last morphology was not detected in the present work due to both the initial chemical composition, in particular the Fe:Mn ratio, and the high cooling rate. The Fe-rich polygonal precipitates have a variable size, up to ten of microns. From the comparison of the size of Fe-bearing particles with the α-Al cell size of the alloys, it is possible to distinguish between primary and secondary (or pro-eutectic) Fe-rich particles.
According to this criterion, coarser Fe-rich precipitates are primary particles that have formed in the holding furnace or during the melt transfer from the casting furnace to the shot sleeve, while finer particles can be identified as pro-eutectic, as formed during the solidification phase of the casting [32].
The presence of high Fe content led also to the formation of several primary plate-like β-Al_5FeSi compounds, especially in alloy E (Figure 10), with a length in the range between 20

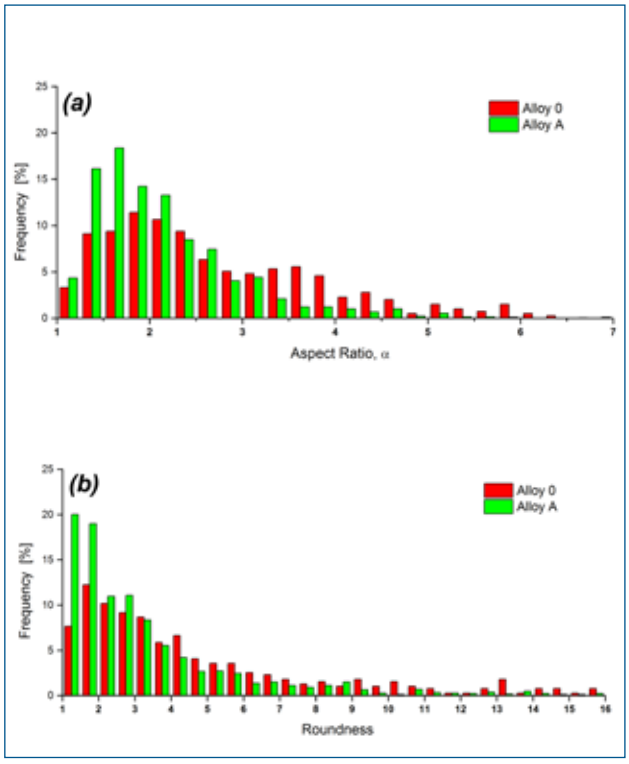

Fig. 8 - Distributions of (a) aspect ratio and (b) roundness of eutectic Si particles in the alloys 0 and A.

Fig. 8 - Distribuzione del rapporto d'aspetto (a) e della rotondità (b) delle particelle di Si eutettico nella lega 0 e nella lega A.

and 30 µm. The high amount of β phase in the alloy E can be attributed to the highest content of Zn and Sr. While the presence of a high Zn concentration decreases the liquidus temperature [10] and promotes the nucleation and growth of primary Fe-rich phases (α and β), the addition of higher Sr content (350 ppm) promotes the formation of plate-like β phase. It is widely reported how, in gravity casting processes, low Sr amount changes the morphology of the Fe-rich

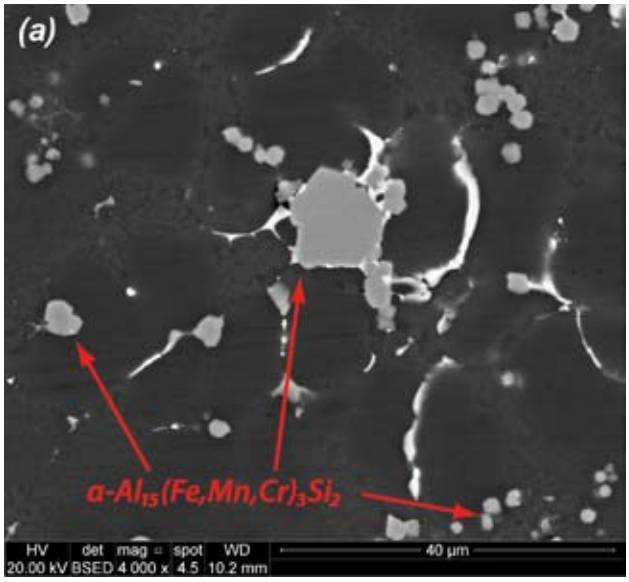

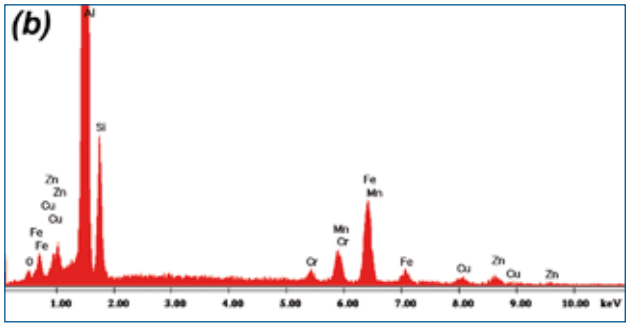

Fig. 9 - (a) SEM micrograph of blocky Fe-rich precipitates and (b) relative EDS spectrum: the presence of Cu and Zn is due to the surrounding α-Al matrix.

Fig. 9 - (a) Micrografia SEM di precipitati poligonali ricchi in Fe e (b) relativo spettro EDS: la presenza di Cu e Zn è dovuta alla matrice α-Al che contiene questi elementi in soluzione solida.

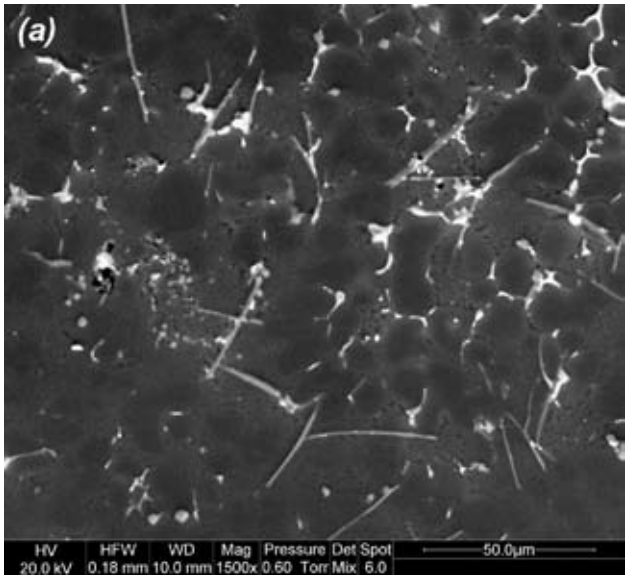

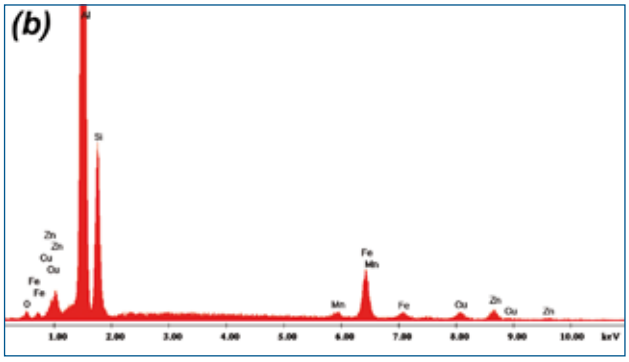

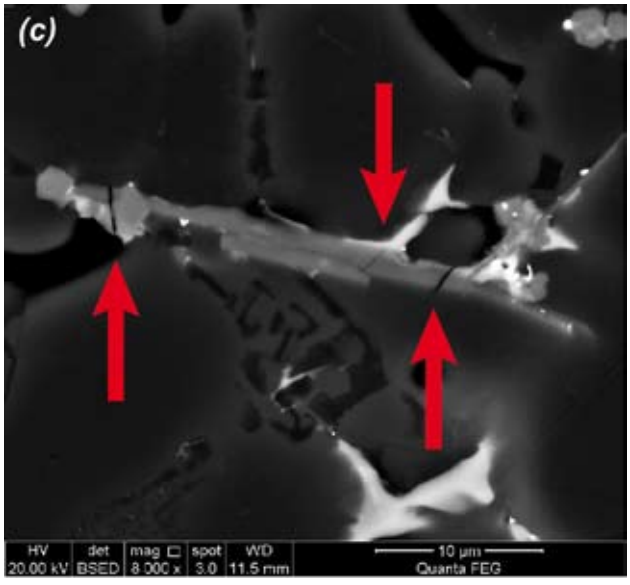

Fig. 10 - (a) SEM micrograph of alloy E where a significant amount of plate-like β-Al_5FeSi particles can be observed. (b) EDS spectrum of a β-Al_5FeSi phase; differently from the spectrum of Figure 9b, Cr is not present. (c) β-phase at high magnification, where the arrows evidence the presence of transversal microcracks.

Fig. 10 - (a) Micrografia SEM della lega E a bassi ingrandimenti: si nota un presenza significativa di precipitati aciculari ricchi in Fe; (b) spettro EDS di una struttura aciculare β-Al_5FeSi: a differenza dello spettro di Fig. 9b non è presente il Cr; (c) precipitato β a elevati ingrandimenti: le frecce evidenziano cricche trasversali.

intermetallics, promoting the formation of α -Fe phase [33]. Contrary, it has been observed that the addition of 0.04 wt.% Sr in a AlSi12 die casting alloy increases the precipitation of primary and secondary β-Al_5FeSi phases [34]. At high magnifications, a series of cracks can be observed in some of the β particles indicating the brittle nature of these intermetallic compounds (Figure 10c).

In addition to the Fe-rich phases, Cu-bearing particles were also detected and characterized as θ-Al2Cu intermetallics. Coarse block-like Al_2Cu particles and lamellar eutectic Al-Al_2Cu structure are present in the interdendritic regions (Figure 11). Further analysis showed the presence of other Mg-rich intermetallic compounds such as the π-$Al_8Mg_3FeSi_6$ and Q-$Al_5Mg_8Cu_2Si_6$ phases, the last with a

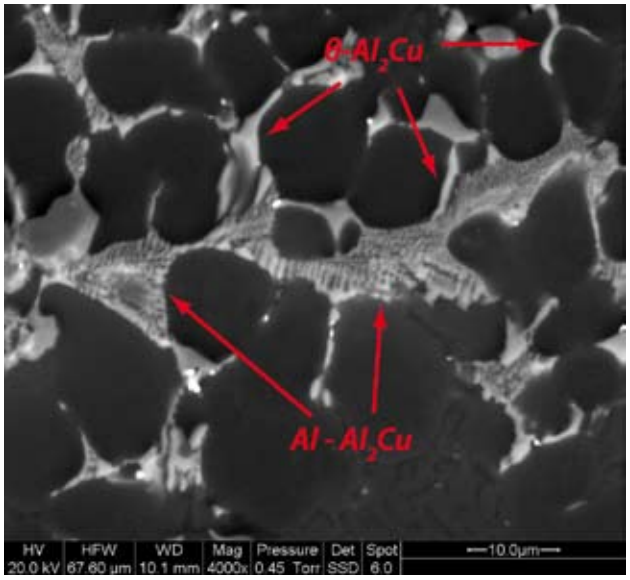

Fig. 11 - SEM micrograph of Cu-bearing particles. Arrows indicate the block-like θ-Al_2Cu particles and the lamellar eutectic Al-Al_2Cu structure.

Fig. 11- Micrografia SEM di precipitati ricchi in rame. Le frecce indicano rispettivamente l'eutettico lamellare Al + θ-Al_2Cu e la fase compatta tipo θ-Al_2Cu.

lamellar morphology as shown in Figure 12. The amount of these two phases is rather limited in the analysed alloys with the exception of the alloy D, where the high concentration of the π and Q phases is due to the highest Mg level (0.68 wt.%).

The volume fraction of coarse intermetallic phases in the different alloys was evaluated on 25 consecutive fields at the centre of the thin sections. The average values are shown in Figure 13 where it can be observed how the volume fraction is considerably influenced by the initial chemical composition of the alloy, in particular by the Cu and Mg levels. The high volume fraction in the alloy E is essentially due to the high amount of coarse β-Al_5FeSi precipitates.

Further EDS analysis carried out in the α-Al matrix evidenced the presence of Si, Mg, Cu and Zn in solid solution or as strengthening precipitates. The cooling rate can influence the saturation of a significant amount of alloying elements in the α-Al matrix. This behaviour is more marked when higher cooling rates take place like at the casting surface, where the formation of coarse intermetallic phases is reduced too.

The TEM observations, associated with the local electron diffraction (SAED, Selected Area Electron Diffraction), confirmed the presence of Fe-rich α phases, in the form of primary and secondary polygonal precipitates (Figure 14a), and the θ-Al_2Cu phase (Figure 14b). Investigations at higher magnifications showed the presence of nanoscale precipitates in the α-Al matrix with a mean size lower than 20 nm (Figure 15).

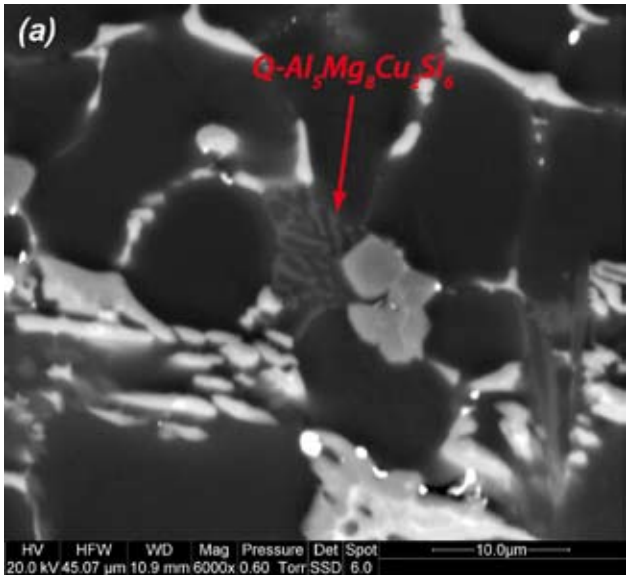

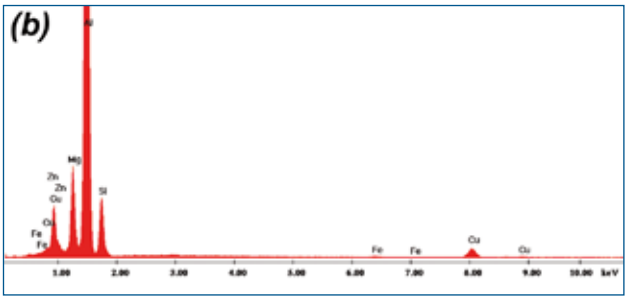

Fig. 12 - (a) SEM micrograph of alloy D where the arrow indicates the Q-$Al_5Mg_8Cu_2Si_6$ phase, as revealed by (b) EDS spectrum.

Fig. 12 - (a) Micrografia SEM della lega D con indicata la fase Q-$Al_5Mg_8Cu_2Si_6$ all'interno di una struttura eutettica; (b) spettro EDS associato alla fase Q.

Mechanical properties

Hardness testing

To investigate the influence of Cu, Mg, Zn and Sr content on the variation in hardness, Brinell hardness and Vickers microhardness measurements were completed on thin section samples. Vickers microhardness measurements were localised in the α-Al crystals. The mean values with the standard deviations are shown in Figure 16. The alloys C and D evidence the highest values in both hardness and microhardness, due to higher Cu and Mg content. These elements are partially dissolved in solid solution within the α-Al matrix and, due to the T1-condition, partially precipitated as secondary phases in the matrix. The increase of hardness through Cu and Mg addition is widely described in the literature [5,35]. Lumley et al. [5] observed how a standard AlSi9Cu3(Fe) die casting alloy shows a hardness value of about 90 HV, while an increase of Cu content, or Cu and Mg together, raise this value at ~100 and ~110 HV, respectively.

Particular attention should be given to the results obtained for the alloy E, which present the lowest Cu (1.90 wt.%)

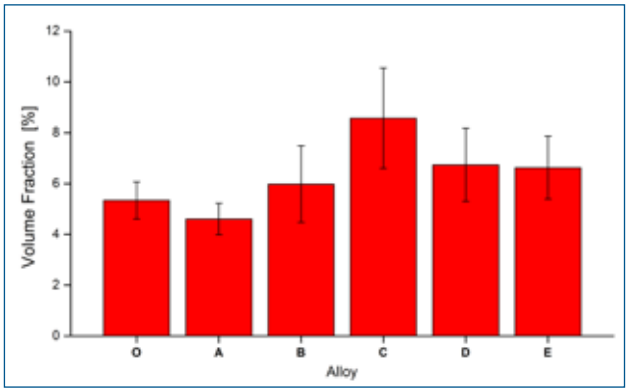

Fig. 13 - Volume fraction of coarse intermetallic phases in the experimental alloys.

Fig. 13 - Frazione volumetrica (%) delle fasi intermetalliche nelle sei leghe oggetto di studio.

and Mg (0.20 wt.%) concentration. The increase of the Zn content up to 4 wt.% permitted to obtain hardness values higher than the alloys 0, A and B, and to reduce at the same time the use of commercially expensive Cu. The microstructural investigation of this alloy did not evidence the presence of coarse Zn-rich intermetallic phases. Due to the high solubility in the Al matrix, Zn is almost completely dissolved in solid solution or present in the form of precipitates in the α-Al matrix. This behaviour leads to the increase of microhardness and hardness, even if, in the second case, the presence of Fe-needle phases has to be taken into account, as previously described. In general, the increase of microhardness given by the addition of Cu, Mg and Zn is related to the distortion of the crystal lattice of the α-Al and to the formation of fine precipitates in the matrix (see Figure 15), which substantially contribute to the strengthening mechanism.
The hardness and microhardness trends observed in the different alloys (Figure 16) show an opposite behaviour to SDAS values (Figure 4). This behaviour, already observed in gravity castings [5,36-39], confirms how the static mechanical properties are closely related to microstructural scale (SDAS) and to the distribution and shape of the eutectic structure.

Tensile testing

The mechanical properties, such as the yield strength ($YS_{0.2\%}$), ultimate tensile strength (UTS), elongation to fracture (ε_r) and static toughness (W_r) of the analysed alloys in their physical state are shown in Figure 17. By analysing the YS, a similar trend to that observed for hardness can be easily noticed. While the standard AlSi9Cu3(Fe) die casting alloy (alloy 0) shows a yield strength of 158 MPa, the addition of both Cu and Mg increases the value up to 208 MPa, with an increment of 30%. The alloy E, where both Zn and Sr were added, shows YS values slightly higher than the base material. The initial yield stress is largely determined by the relatively high supersaturation of atoms (Mg, Cu, Zn and Si), referred to the high solidification rate, and

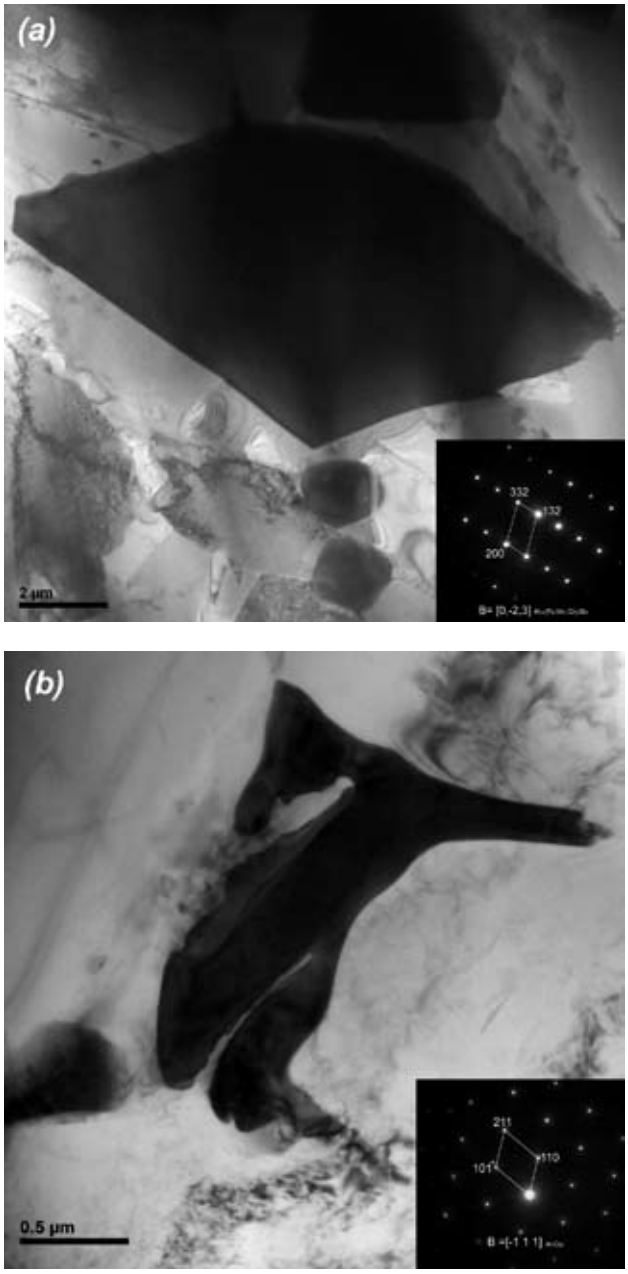

Fig. 14 - TEM micrographs of (a) primary and secondary polygonal precipitates identified as α-$Al_{15}(Fe,Mn,Cr)_3Si_2$, as revealed by the diffraction pattern, and (b) θ-Al_2Cu phase.

Fig. 14 - (a) Micrografia TEM di precipitati poligonali primari e secondari; il pattern di diffrazione, associato al precipitato centrale, lo identifica come α-$Al_{15}(Fe,Mn,Cr)_3Si_2$; b) Micrografia di un precipitato θ-Al_2Cu di una struttura eutettica.

the precipitation hardening of secondary phases in the α-Al matrix.
The UTS seems to vary around ~280 MPa and the small variations, visible in Figure 17, among the experimental alloys can be associated to the different defect content, especially porosity normally present in die casting. However, the highest UTS was observed for the alloy C (303 MPa), which presents the higher Cu level, while the lowest

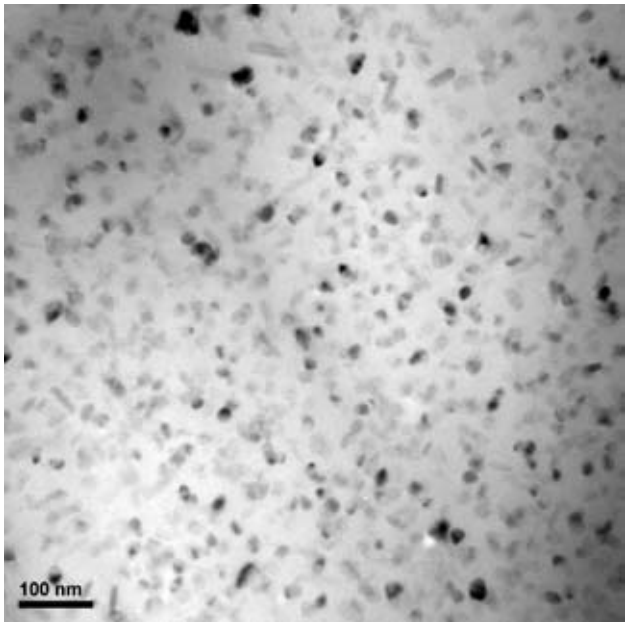

Fig. 15 - TEM micrograph of strengthening precipitates within the α-Al matrix.

Fig. 15 - Immagine TEM di precipitati nanometrici presenti all'interno della matrice α-Al.

value was for the alloy E (235 MPa). The Zn and Sr addition, as previously described, promotes the formation of brittle plate-like Fe-rich compounds (β-Al_5FeSi), which has an impact on the ultimate tensile strength and a deleterious effect especially on the elongation to fracture. For this reason the formation of the α-$Al_{15}(Fe,Mn,Cr)_3Si_2$ phase instead of the β-phase is preferred.

The elongation to fracture is the most sensitive mechanical parameter with the greatest variations among the analysed alloys (Figure 17). The addition of Sr to the base alloy greatly improves the value of ε_r, due to the modification of the eutectic Si particles, which become finer and fibrous. In this way fewer stress concentration points arise in the microstructure. The benefits given by Sr addition vanished, however, with further addition of alloying elements (Cu, Mg and Zn), which allow to increase the yield strength by reducing the ductility.

The static toughness (W_r), that is the ability of the material to store energy in the elastic-plastic field before fracture, was also studied from tensile testing. This value is shown in Figure 17 and it is related to the area under the engineering stress-strain curve, which can be approximated as proportional to the ultimate tensile strength and the elongation to fracture [40]:

$$W_r = \frac{W_{tot}}{V_0} = \int_0^{\varepsilon_r} \sigma \, d\varepsilon \quad \propto \quad UTS \cdot \varepsilon_r \qquad (3)$$

Other mechanical properties such as the strain hardening exponent n and the strength coefficient K (MPa), which are related to the true stress and the true plastic strain according to the Hollomon equation [41], were analysed (Figure

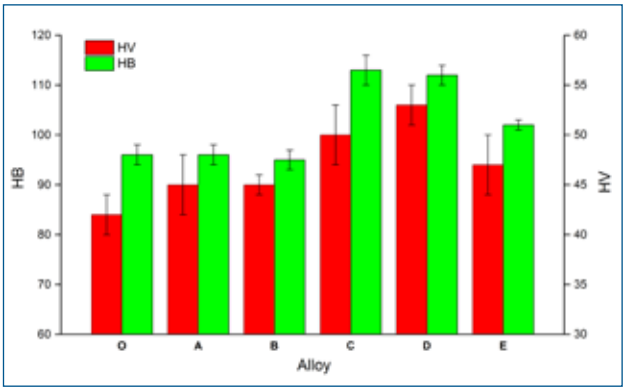

Fig. 16 - Brinell hardness (HB) and Vickers microhardness (HV) of the analysed alloys. Data refer to the thin sections drawn from the castings. Standard deviations are given as error bars.

Fig. 16 - Andamento della durezza Brinell (HB) e microdurezza Vickers (HV) per le diverse leghe analizzate. I dati fanno riferimento alle sezioni di spessore sottile. Le barre di errore rappresentano la deviazione standard.

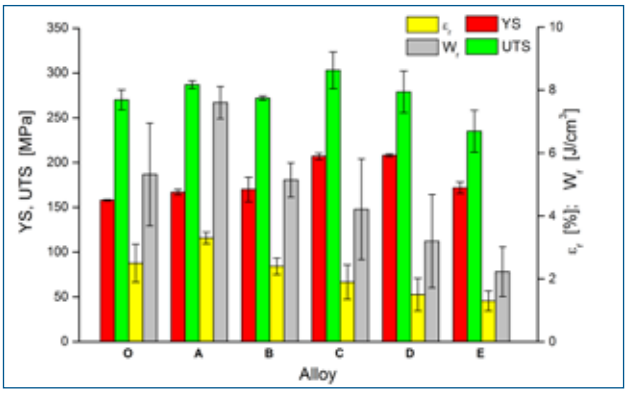

Fig. 17 - Average YS, UTS, elongation to fracture (ε_r), and static toughness (W_r) in the experimental alloys. Standard deviations are given as error bars.

Fig. 17 - Valori medi della tensione di snervamento (YS), del carico (UTS) e dell'allungamento a rottura (ε_r), e della tenacità statica (W_r) per le varie leghe analizzate. Le barre di errore rappresentano la deviazione standard

18). The variation of these two parameters reflects some considerations previously done. The parameter n is a measure of the ability of the material to strain harden; the larger its magnitude, the greater the strain hardening for a given amount of plastic strain. K is a measure of the ability of a material to withstand deformation. The values of n and K varies from one alloy to another and also depend on the temper of the material. Generally, a diecast alloy that tolerates higher plastic deformations without incurring in necking presents a high value of n. It follows, from the present results, that the die casting alloys with a high content of Cu and Mg (alloys C and D), which present the highest strength values, show lower strain hardening exponents if compared to the base alloy.

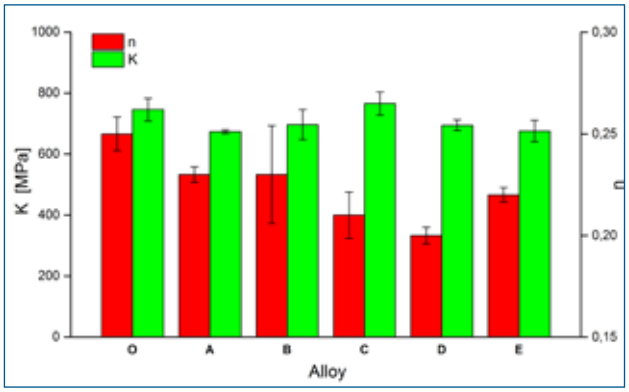

Fig. 18 - Average strain hardening exponent, n, and strength coefficient, K, for the analysed alloys. Standard deviations are given as error bars.

Fig. 18 - Valori medi dei coefficienti di incrudimento (n) e di resistenza (K) per le varie leghe analizzate. Le barre di errore rappresentano la deviazione standard

CONCLUSIONS

The effect of different alloying elements such as Cu, Mg, Zn and Sr on microstructural and mechanical properties of a high-pressure diecast AlSi9Cu3(Fe) steering gearbox has been investigated. Based on the results obtained in the present study, the following conclusions can be drawn.

- The microstructural scale, evaluated with SDAS, depends on both the local cooling rate and the initial chemical composition of the alloy.
- The SDAS decreases with the addition of Cu, Mg and Sr, while it increases by adding Zn.
- The porosity amount, in particular the macroshrinkage, is reduced with the addition of 4 wt.% Cu.
- The Sr-modification on eutectic Si has greater effect when low levels of Cu, Mg and Zn are present.
- The presence and amount of different intermetallic phases strictly depend on the initial chemical composition. Increasing the level of Cu and Mg in the alloy, Cu- and Mg-rich compounds (θ, Q, π) proportionally increase. Further, high levels of Zn (4 wt.%) and Sr (350 ppm) induce the formation of β-Al_5FeSi phase.
- Cu and Mg, especially if combined together, are the alloying elements that mainly reinforce the material through solid solution strengthening and fine precipitation hardening into the α-Al matrix.
- The yield stress is positively influenced by the increasing the Cu and Mg levels, while the ductility and the toughness assume the highest values with the sole addition of Sr.

Acknowledgements

The authors would like to thank ZML Industries SpA (Maniago, PN) for high-pressure die casting of the steering gearboxes and in particular Ing. F. Doria for the useful support to the present research. Many thanks are also due to P.I. G. Mazzacavallo (DTG) and Dr. E. Della Rovere (DTG) for the experimental contribution to this work.

REFERENCES

[1] D. Apelian, M.M. Makhlouf, High Integrity Aluminium Die Casting: Alloys, Processes and Melt Preparation. North American Die Casting Association, Des Plaines, IL (2004) 1-14.
[2] X. Dai, X. Yang, J. Campbell, J. Wood, Mater. Sci. Technol. 20 (2004) 505-513.
[3] G. Timelli, F. Bonollo, Metal. Sci. Tech. 26 (2008) 2-8.
[4] M.M. Makhlouf, D. Apelian, L. Wang, Microstructures and properties of aluminium die casting alloys, NADCA, Rosemont, Illinois, USA (1998).
[5] R.N. Lumley, R.G. O'Donnell, D.R. Gunasegaram, M. Givord, Metall. Mat. Trans. A 38 (2007) 2564-2574.
[6] R.N. Lumley, R.G. O'Donnell, D.R. Gunasegaram, T. Kittel-Sherri, M. Gershenzon, A.C Yob, I.J. Polmear, Metal. Sci. Tech. 26 (2008) 2-11.
[7] R.E. Spear, G.R. Gardner, AFS Trans. 71 (1963) 209-215.
[8] C.H. Càceres, C.J. Davidson, J.R. Griffiths, Mater. Sci. Eng. A 197 (1995) 171-179.
[9] M. Merlin, Metall. Ital. 3 (2010) 37-47.
[10] S. Gowri, F.H. Samuel, Metall. Mat. Trans. A 25 (1994) 437-448.
[11] J.G. Kaufman, E.L. Rooy, Aluminum Alloy Castings: Properties, Processes and Applications, ASM International, (2004).
[12] L. Ceschini, I. Boromei, A. Morri, S. Seifeddine, I. L. Svensson, J. Mat. Proc. Tech. 209 (2009) 5669-5679.
[13] P.N. Crepeau, AFS Trans. 103 (1995) 361.
[14] T.O. Mbuya, B.O. Odera, S.P. Nganga, Int. J. Cast Met. Res. 16 (2003) 451-465.
[15] M.V. Kral, H.R. McIntyre, M.J. Smillie, Scripta Mater. 51 (2004) 215-219.
[16] S.G. Shabestari, Mater. Sci. Eng. A 383 (2004) 289-298.
[17] G. Timelli, E. Fiorese, Metall. Ital. 3 (2011) 9-23.
[18] S. Seifeddine, I.L. Svensson, Proc. 4th Int. Conference High Tech Die Casting, Montichiari, 09-10 April 2008.
[19] J.R. Brown, Foseco Non-Ferrous Foundaryman's Handbook, 11th ed., Butterworth-Heinemann, Oxford, UK, 1999.
[20] Q. G. Wang, D. Apelian, D. A. Lados, J. Light Met. 1 (2001) 85-97.
[21] J. Campbell: "CASTINGS, The new metallurgy of cast metals" II edition, Butterworth-Heinemann Edition, 2003.
[22] M. Conserva, F. Bonollo, G. Donzelli: "Alluminio manuale degli impieghi"; ed. Edimet (2004).
[23] T. Sivarupan, C.H. Càceres, J.A. Taylor, Effect of composition on secondary dendrite arm spacing of Al-Si-Cu-Mg (Fe/Mn) alloys for a given cooling rate, The University of Queensland Engineering Post Graduate School Conference – 2011.
[24] M. B. Djurdjevič, M. A. Grzinčič, Archives of Foundry Engineering 12 (2012) 19-24.
[25] W. Kurz, D.J. Fisher, Fundamentals of Solidification, Trans Tech Publications (1986).
[26] U. Feurer, Quality Control of Engineering Alloys and the Role of Metals Science, Delft University of Technology, (1978), 131.
[27] M. Easton, C. Davidson, D. St John, Metall. Mat. Trans. A 41 (2010) 1528-1538.
[28] E. Tillová, M. Chalupová, L.Hurtalová, Evolution of Phases in a Recycled Al-Si Cast Alloy During Solution Treatment in Scanning Electron Microscopy, Edited by Viacheslav Kazmiruk, InTech, (2012).
[29] M.M. Makhlouf, Proc. 8th Int. Summer School on Casting and Solidification of Aluminium- and Magnesium Alloys, Trondheim, NO (2006).
[30] L. Heusler, W. Schneider, J. Light Met. 2 (2002) 17-26.
[31] L. Backerud, G. Chai, J. Tamminen, Solidification Characteristics of Aluminum Alloys-vol.II: Foundry Alloys. American Foundrymen's Society Inc., IL (1990).
[32] J.L. Jorstad, Die Cast. Eng. 11/12 (1986) 30-36.
[33] M.H. Mulazimoglu, A. Zaluska, J.E. Gruzleski, F. Paray, Metall. Mat. Trans. A 27 (1996) 929-936.
[34] B. Suárez-Peña, J. Asensio-Lozano, Scripta Mater. 54 (2006) 1543-1548.
[35] M. Zeren, E. Karakulak, S. Gumu, Trans. Nonferrous Met. Soc. China 21 (2011) 1698-1702.
[36] M. Tiryakioglu, J. Campbell, J.T. Staley, Scripta Mater. 49 (2003) 873-878.
[37] Q.G. Wang, C.H. Cáceres, Metall. Mat. Trans. A 241 (1998) 72-82.
[38] Q.G. Wang, Metall. Mat. Trans. A 34 (2003) 2887-2899.
[39] S.G. Shabestari, F. Shahri, J. Mat. Sci. 39 (2004) 2023-2032.
[40] T.H. Courtney, Mechanical Behavior of Materials, McGraw-Hill, New York (1990) 70-79. H.J. Kleemola, M.A. Nieminen, Metallurgical Transactions, 5 (1974) 1863-1866.

Caratterizzazione multiscala di leghe AlSi9Cu3(Fe) pressocolate dopo alligazione con Cu, Mg, Zn e Sr

Parole chiave: **Alluminio e leghe – Solidificazione – Precipitazione – Pressocolata - Prove Meccaniche – Metallografia – Difettologia - Prove Non Distruttive**

Le leghe della famiglia Al-Si sono diventate negli ultimi anni le più diffuse in commercio e costituisco ormai il 90% delle leghe di alluminio impiegate nel settore automotive. Tra i processi industriali destinati alla produzione di componenti in lega di alluminio, la pressocolata è senza dubbio la tecnologia più diffusa. Tuttavia questo processo, pur mostrando molti vantaggi, induce difettosità nei componenti, quali inclusioni e porosità, che ne compromettono le caratteristiche meccaniche. Adottando pratiche fusorie più efficienti e migliorando l'approccio in fase di progettazione del componente è possibile ridurre il tenore di difetti, migliorando di conseguenza la resistenza del componente stesso. Le proprietà meccaniche possono essere inoltre sensibilmente incrementate dalla variazione di alcuni parametri microstrutturali quali la distanza fra i bracci secondari delle dendriti (SDAS), la dimensione della grana cristallina, la forma e la distribuzione dell'eutettico alluminio-silicio e la frazione volumetrica delle fasi intermetalliche. Queste caratteristiche microstrutturali, oltre a dipendere dalle condizioni di solidificazione, sono strettamente legate alla composizione chimica della lega utilizzata e possono essere influenzate dall'eventuale aggiunta di elementi modificanti come Na e Sr. Anche altri elementi, come Cu, Mg, Si, Zn, Fe, Mn, che normalmente sono presenti nelle leghe di Al da pressocolata, influenzano la microstruttura del materiale, e di conseguenza le proprietà meccaniche.
Generalmente, nel settore automotive viene richiesta una pluralità di caratteristiche che difficilmente può essere soddisfatta con l'impiego di una lega di alluminio secondaria standard. Spesso la tendenza è quella di modificare la microstruttura del materiale agendo sulla composizione chimica della lega tramite l'aggiunta di opportuni elementi chimici, al fine di ricercare nuovi e più ampi "compromessi" sulle prestazioni del materiale.
In questo lavoro viene discussa l'influenza di alcuni elementi alliganti quali Cu, Mg, Zn e Sr sulla microstruttura e sulle proprietà meccaniche di getti pressocolati destinati al settore automotive realizzati in lega AlSi9Cu3(Fe) (EN AC 46000).
Le indagini metallografiche eseguite tramite microscopia ottica ed elettronica a scansione e a trasmissione hanno permesso di valutare a scale differenti la dimensione dei cristalli primari di α-Al e delle porosità, nonché di identificare le diverse fasi intermetalliche presenti.
I risultati sperimentali ottenuti mostrano che la spaziatura tra i rami secondari delle dendriti dipende sia dalla composizione chimica, sia dalla velocità di raffreddamento. A parità di spessore del getto lo SDAS diminuisce con l'aggiunta di elementi in lega (Sr, Cu, Mg). Un effetto opposto si riscontra invece per lo Zn, poiché esso abbassa la temperatura di liquidus, favorendo di conseguenza l'accrescimento dendritico (Fig. 5).
Variando la composizione chimica della lega EN AC 46000 è stata diminuita la presenza di macroporosità nei getti prodotti, in particolare con l'aggiunta del 4%pond di Cu (Fig. 3). Viceversa si è osservato che la modifica del Si eutettico effettuata con Sr ha una efficacia maggiore quando la lega presenta una bassa concentrazione di Cu, Mg o Zn (Fig. 6).
La tipologia e la quantità di fasi intermetalliche presenti sono legate al tenore degli elementi alliganti aggiunti in lega, ad eccezione dello Sr, che agisce principalmente come elemento modificante. All'aumentare di Cu e Mg, aumentano proporzionalmente le fasi intermetalliche ricche di questi elementi (θ, Q, π) (Fig. 11-12). Inoltre elevati tenori di Zn (4%) e Sr (350 ppm) inducono la formazione di fasi β-Al_5FeSi (Fig. 10).
Le prove di durezza e di microdurezza hanno evidenziato che Cu e Mg, soprattutto se combinati tra loro, sono gli elementi che maggiormente rafforzano il materiale (Fig. 16). Essi infatti riducono le dimensioni dello SDAS, promuovono la formazione di un maggior numero di fasi indurenti e rafforzano la matrice α-Al, tramite soluzione solida e precipitazione di fase. Risultati simili si sono ottenuti dall'analisi delle prove di trazione. La tensione di snervamento è positivamente influenzata dall'aggiunta combinata di Cu e Mg, mentre l'allungamento a rottura e la tenacità assumono i valori massimi con la sola aggiunta di stronzio (Fig. 17).